Directly Addressable Sub-3 nm Gold Nanogaps Fabricated by Nanoskiving Using Self-Assembled Monolayers as Templates

Parisa Pourhossein and Ryan C. Chiechi*

Stratingh Institute for Chemistry, and Zernike Institute for Advanced Materials, University of Groningen, Nijenborgh 4, 9747 AG Groningen, The Netherlands

ABSTRACT

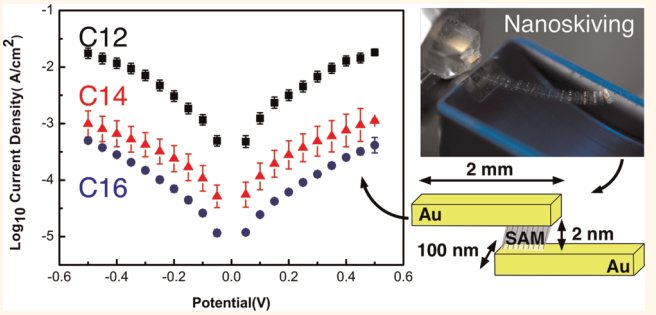

This paper describes the fabrication of electrically addressable, high-aspect-ratio (>10000:1) nanowires of gold with square cross sections of 100 nm on each side that are separated by gaps of 1.7−2.2 nm which were defined using self-assembled monolayers (SAMs) as templates. We fabricated these nanowires and nanogaps without a clean room or any photo- or electron-beam lithographic processes by mechanically sectioning sandwich structures of gold separated by a SAM using an ultramicrotome. This process is a form of edge lithography known as Nanoskiving. These wires can be manually positioned by transporting them on drops of water and are directly electrically addressable; no further lithography is required to connect them to an electrometer. Once a block has been prepared for Nanoskiving (which takes less than one day), hundreds of thousands of nanogaps can be generated, on demand, at a rate of about one nanogap per second. After ashing the organic components with oxygen plasma, we measured the width of a free-standing gap formed from a SAM of 16-mercaptodohexanoic acid (2.4 nm in length) of 2.6 ± 0.5 nm by transmission electron microscopy. By fitting current−voltage plots of unashed gaps containing three alkanedithiolates of differing lengths to Simmons' approximation, we derived a value of $\beta = 0.75$ Å^{-1} (0.94 n_C^{-1}) at 500 mV. This value is in excellent agreement with literature values determined by a variety of methods, demonstrating that the gap-size can be controlled at resolutions as low as 2.5 Å (*i.e.*, two carbon atoms).

KEYWORDS: nanoskiving · nanogaps · molecular electronics · self-assembled monolayers · nanofabrication

A central challenge to electrically interfacing molecules from our macroworld is producing nanostructures that possess both features on the molecular scale—single nanometers—and on a scale large enough to connect to external circuitry.[1,2] Several methods of fabricating nanoscale gaps with controlled spacing have been reported, including mechanical break junctions,[3] electron-beam lithography,[4] electrochemical plating,[5,6] electromigration,[7] focused ion beam lithography,[8] shadow evaporation,[9] scanning probe and atomic force microscopy,[10] on-wire lithography,[11] and molecular rulers.[12] Each of these methods have their own applications and limitations, but despite all the progress in this field, there remain challenges to producing electrodes with single-nanometer spacings that can be fabricated and positioned in a precise and controllable manner and that are readily electrically addressable. The most common approach is to fabricate the "nano" part of the device, containing a nascent gap (*e.g.*, the sacrificial metal in on-wire lithography or the constriction point in break junctions) and then using a lithographic process to connect it to wires and contact pads before unmasking the nanogap. This approach is effective, but laborious, and because gap-sizes of single nanometers also demand subnanometer resolutions, they push modern nanofabrication methods to their technical limits. The resulting complexity necessitates specialized infrastructure (clean rooms, e-beam/photolithography equipment, *etc.*) and the commensurate overhead—cost, training, and time. A more desirable approach is to start from a simple technique that is far from its technical limits, leaving plenty of room for improvement and adaptation to specific experiments/applications.

Nanoskiving is an emerging technology for nanofabrication. It is based on edge lithography and uses an ultramicrotome to mechanically section thin films using a diamond knife that is attached to a metal "boat" full of water.[13−15] The thin-film structure is embedded in a block of epoxy that is then pushed onto the edge of the diamond knife, advancing each time by a set amount that defines the thickness of each section. The resulting slab of epoxy contains the

* Address correspondence to r.c.chiechi@rug.nl.

Received for review April 5, 2012 and accepted May 11, 2012.

Published online May 11, 2012
10.1021/nn301510x

cross-section of the thin film and floats on the surface of the water in the boat. Successive sections stick together by hydrophobic interactions creating a "ribbon" of nanostructures that can be transferred either all-together or one-at-a-time to a substrate *via* a drop of water. The slabs can also be aligned magnetically (by incorporating nickel into the epoxy) as the water evaporates, allowing the sections to be placed and oriented as desired.[16] Nanoskiving is particularly useful for generating nanostructures comprising more than one material[17] because the process is mechanical and therefore compatible with soft materials such as conjugated polymers[18,19] and delicate organic compounds that would not survive the etching and development steps of conventional e-beam/photolithography. And edge lithography lends itself to creating structures with high aspect ratios, which is ideal for producing nanogaps that are directly addressable. Nanoskiving is also simple and fast, requiring no special infrastructure such as clean rooms or semiconductor fab tools and it produces nanostructures on-demand. In principle, Nanoskiving does not even require electricity, sans the minute amount consumed by the electric motors that advance the block toward the knife.

RESULTS/DISCUSSION

Fabrication. We are particularly interested in the application of nanogap structures to construct metal−molecule−metal tunneling junctions, where molecules are placed between electrodes through which they can be addressed from the macroworld. There are three general approaches to addressing molecules electrically: (i) forming gaps in electrode materials that are on the same length scale as the molecules of interest and then allowing (typically only a few of) these molecules to self-assemble into the gaps; (ii) forming SAMs and then applying a top-contact; and (iii) forming monolayers parallel to the surface of nanogap electrodes.[20,21] We combined these approaches by forming SAMs on thin films (100 nm) of gold, evaporating a second layer of gold (100 nm) to form a gold/SAM/gold sandwich, and then slicing thin sections (50−100 nm) perpendicular to the plane of the SAM by Nanoskiving. The resulting structures comprise two nanowires separated by the smallest dimension of a SAM. This method circumvents the high frequency of electrical shorts (~98.8% for alkanthiolates on gold[22]) that normally results from depositing metal contacts directly onto SAMs because the total area of the skived SAM is only ~50 μm^2.[23] (For comparison, liquid Ga−In contacts yield 85−90% working junctions and are ~1000 μm^2, while liquid Hg contacts are 10× larger and yield <50%.[24,25]) Nanoskiving has been used in combination with photolithographic techniques to produce electrically addressable

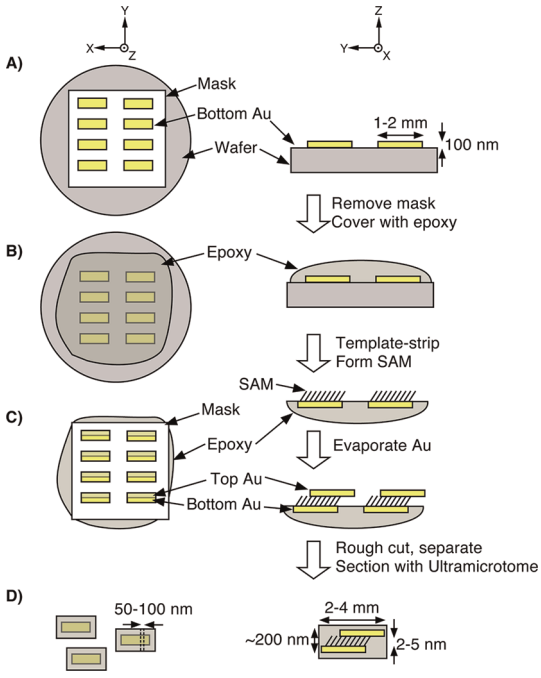

Figure 1. A schematic (not to scale) of the fabrication of STAN electrodes. The left column is the top-down view and the right column is the side-view. (A) A 100 nm-thick layer of gold is deposited through a Teflon shadow mask onto a fluorinated silicon wafer *via* thermal evaporation to produce an array of millimeter-sized rectangles. (B) The mask is removed and the gold features covered in epoxy. After the epoxy cures, it is separated from the wafer such that the gold features remain adhered to the epoxy. A SAM is then formed on the newly exposed gold surfaces. (C) The Teflon mask is placed over the SAM-covered gold features with an offset of 250−500 μm and another 100 nm-thick layer of gold is deposited. (D) The mask is removed and the gold/SAM/gold features are separated by rough-cutting the epoxy with a jeweller's saw. The features are then embedded in epoxy and sectioned with an ultramicrotome.

nanowires separated by a 30 nm-thick layer of SiO_2,[26] but applications in tunneling junctions require gaps below 10 nm. In addition, we greatly simplified the fabrication process and eliminated the use of photolithography by simply offsetting the evaporated gold features by hand. The entire procedure is summarized in Figure 1. A silicon wafer is cleaned with an air plasma and then passivated with a perfluorinated trichlorosilane. Rectangles of gold (1−2 mm) are deposited by evaporation through a Teflon mask. Epofix epoxy prepolymer is poured over the entire wafer, covering the gold features, and the epoxy is cured before being template-striped[27] by separating the epoxy from the wafer; the gold features remain adhered to the epoxy. A SAM is formed by submerging these features in a 1 mM ethanolic solution of the appropriate thiol overnight. A second set of gold rectangles is deposited by placing the Teflon shadow mask over the SAM-covered gold features with an offset of 250−500 μm with respect to the first evaporation. This offset will eventually define the longest dimension of the gap, and it can be accurately measured using a microruler before

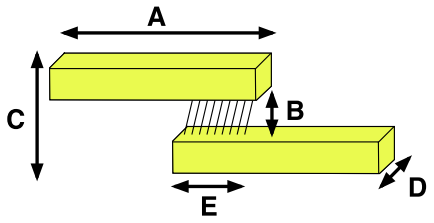

Figure 2. A schematic (not to scale) of the dimensions of the STAN electrodes showing how each dimension is defined. (A) The length of each wire is defined by the shadow mask. (B) The size of the gap between the wires is defined by the thickness of the SAM. (C) The total width is defined by the two gold deposition steps. (D) The depth is defined by the ultramicrotome. (E) The amount of overlap—and the longest dimension of the nanogap—is defined by the offset between the first and second gold-deposition steps.

embedding the entire structure in epoxy for sectioning. Figure 2 is a schematic of the resulting SAM-templated addressable nanogaps (STANs) and how each dimension is defined; the longest dimension by the shadow mask, the smallest (the gap) by the thickness of the SAM, the width by the ultramicrotome, and the thickness by the evaporation of the gold.

The resulting structures are 2−4 mm in total length, but since the length of the gap (dimension E from Figure 2) is only 250−500 μm, 0.75−1.75 mm of each wire is available for electrical contact, obviating the need for further lithography to connect the wires to an electrometer. The gold wires have square cross sections of only 100 nm on a side and are therefore too fragile to directly contact using a probe station; however, contact pads can be applied by hand using small drops of a liquid conductor such as silver paste or conductive carbon paint. We used a combination of silver paste and micrometer-sized tips of eutectic Ga−In (EGaIn) formed at the tip of a syringe.[28] The ability to pick-and-place nanogaps and then contact them directly is unique to STAN electrodes. The typical trade-off between directly fabricating nanogaps *via* photo/e-beam lithography and forming them *via* chemical process in a template is that the former allows the gaps to be fabricated in-place, but is constrained by the resolution of lithography, while the latter may produce large numbers of gaps, but they must be addressed one-at-a-time using e-beam lithography to form contact pads. Nanoskiving falls somewhere between; STAN electrodes are fabricated serially at a rate of ~1 s^{-1} and each block can produce hundreds of thousands of STAN electrodes (and the blocks are fabricated dozens at a time). The individual sections can be placed onto arbitrary substrates (that are sufficiently wetted by water) with control over position and orientation, or they can be transferred from the boat as a ribbon of several sections by dipping a substrate into the water and slowly raising it from underneath the ribbon (see Supporting Information for a photograph of a ribbon). Although we use silver paste for convenience, it is by no means necessary; the STAN structures could, for example, be placed onto predefined contact pads. Gaps of different sizes can also be combined onto one substrate simply placing different STAN structures next to each other. Thus, hundreds of nanogaps of various sizes can be fabricated, positioned, and wired up by hand, in a matter of minutes, and directly on the benchtop. Our average fabrication rate was 12 seconds per completed device, from sectioning to connection to the electrometer (excluding oven-drying and acquiring *I*/*V* curves, which are nonserial processes). The fabrication process presented in this paper also represents the low end of complexity for Nanoskiving and utilizes a commercial ultramicrotome that is designed neither for high throughput nor automation.

Electron Microscopy. We initially prepared STAN electrodes of four different gap-widths, one using hexadecane-1,16-dithiol (SC16S), one using tetradecane-1,14-dithiol (SC14), one using dodecane-1,12-dithiol (SC12S), and one using hexane-1-thiol (SC6). The end-to-end (S−S for the dithiols and S−C for SC6) length of each molecule in the extended (AM1 minimized) conformation is 21.7, 19.7, 17.0, and 7.8 Å respectively. In principle the SAMs of these molecules will produce STANs with gaps-widths of the hypotenuse formed from these lengths and the tilt-angle of the respective SAM on gold; however, SAMs of SC6 are disordered and liquid-like at room temperature, while SC12S, SC14S, and SC16S form well-ordered, (liquid) crystalline SAMs.[29] Moreover, the methyl-terminated SAMs of SC6 will likely have a lower-energy interaction with gold than the thiol-terminated SAMs of SC12S, SC14S, and SC16S. Thus, if the SAMs are able to template nanogaps, we have three expectations: (i) SAMs of SC6 should not produce a gap; (ii) both SC16S and SC12S should form gaps and these gaps should be stable due to the stronger interaction of thiols with gold;[30] and (iii) the gaps produced by SC16S, SC14S, and SC12S should differ in size. This last expectation is experimentally challenging to observe, as the difference in widths of the gaps is expected to be less than one nanometer. While it is preferable to image the STAN structures as-fabricated, due to excessive charging of the Epofix resin, we had to ash the organics (including, presumably, the SAMs) using an oxygen plasma (~15 min) before imaging by SEM; representative electron micrographs are pictured in Figure 3. There is no visible gap between the gold wires formed using SC6, implying that the liquid-like SAM was readily penetrated by the evaporated gold; however, the gaps formed from

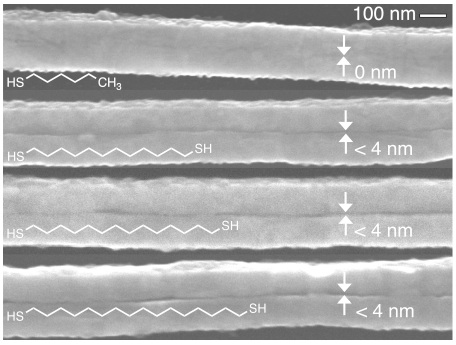

Figure 3. Scanning electron micrographs of the gaps of four different STAN electrodes prepared using different thiols as templates, after ashing the organics with oxygen plasma. From top to bottom: SC6 results in no visible separation between the two gold wires; SC12S shows a clearly visible gap; SC14S shows a clearly visible gap that is qualitatively larger than the gap formed by SC12S; SC16S shows a clearly visible gap that is qualitatively larger than the gaps formed by SC12S and SC14S. All three of the gaps formed by SAMs of dithiols are below the resolution limit of the instrument (~4 nm), thus they are labeled as "<4 nm".

SC16S, SC14S, and SC12S are clearly visible, and the size of the gap appears to increase with the length of the molecule. The resolution limit of the SEM, however, precluded the accurate measurement of features below ~4 nm. Thus, we conclude that the gap-width of these STANs is <4 nm. The gaps and total length of the wires cannot be resolved simultaneously (*i.e.*, at one magnification), but series of images across the STAN structures reveal uniform wires and gaps. An SEM image of the edge of the overlap between two wires is shown in the Supporting Information. Efforts to measure the gaps precisely using AFM, CP-AFM, and STM failed due to either the extreme aspect-ratios of the STANs and, for unashed STANs, the disparate properties of the materials (*i.e.*, gold, alkanedithiols, and epoxy).

To determine whether the gaps extended through the entire thickness of the STANs, we prepared STANs that were 50 nm thick (dimension D from Figure 2) to reduce the aspect ratio, and imaged them by TEM. For the gaps containing SC12S, SC14S, and SC16S, aligning the samples perfectly perpendicular to the electron-beam proved too challenging; these gaps are on the order of the wavelength of an electron and have an aspect-ratio of 50:1 (height:width). In addition to the SAMs of dithiols, we fabricated STANs using 16-mercaptohexadecanoic acid ($SC15CO_2H$), which forms dense SAMs that are mechanically stable (due to internal hydrogen-bonding). We were able to resolve the gaps of these STANs more readily by SEM than the gaps from the dithiols due to the apparent poor adhesion of gold to the terminal carboxylic acid groups, which allowed one wire to shift slightly with respect to the other, making the sharp edges of the gaps clearer by electron microscopy and therefore easier to measure. The top image in Figure 4 is an

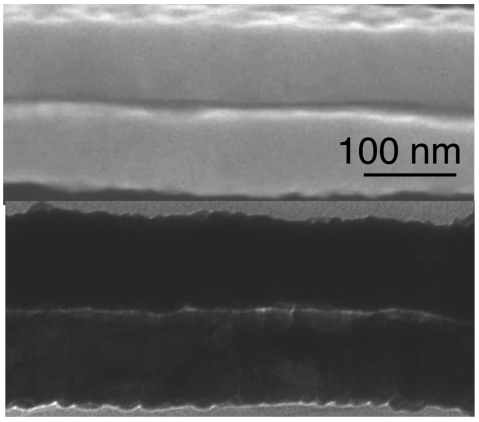

Figure 4. Scanning (top) and transmission (bottom) electron micrographs of gaps formed using 1-mercaptohexadecanoic acid, after ashing the organics with oxygen plasma. The light region in the bottom (TEM) image shows that the gap extends through the entire thickness of the gold wires (100 nm). The width of this light region is 2.6 ± 0.5 nm. The gap in the top (SEM) image appears to be significantly larger than 2.6 nm because the wires are tilted slightly downward, and are offset slightly, creating a high contrast between sharp edge of the lower wire (the cross section of the wires is rectangular) and the shadow from the upper wire.

SEM of a STAN fabricated from $SC15CO_2H$ in which the edge of the lower electrode appears brighter than the face, drawing a sharp contrast with the gap, which appears dark. We were able to image the gap of one of these STANs by TEM (Figure 4; bottom) as well, from which we calculated a width of 2.6 ± 0.5 nm by comparing the pixel intensity *versus* displacement from five different regions distributed across the STAN structure. (The clarity of the gap is remarkable given the challenges of unambiguously resolving TEM images of gaps below 10 nm.[31]) More importantly, the TEM image shows that the gap extends through the entire thickness of the STAN, which implies that the deposited gold did not penetrate the SAM sufficiently to form filaments and that free-standing STANs (*i.e.*, after ashing the organics with oxygen plasma) with gaps of ~3 nm are mechanically stable.

Electrical Measurements. The disparate dimensions of STAN structures—nanometers in two dimensions and millimeters in the third—make it impossible to directly image them in their entirety. Electrical measurements, however, provide an indirect estimate of the size of a nanogap, provided the emission area can be estimated reasonably; we can measure the largest dimension (E from Figure 2) directly, and the other (D from Figure 2) is defined by the ultramicrotome. To measure the *J*/*V* characteristics, we made electrical contact by placing the epoxy sections containing STAN electrodes on a clean SiO_2 substrate and then applying drops of silver paste to each electrode under a light microscope. (While the electrodes themselves are too small to visualize, the index mismatch between the epoxy slab and gold nanostructures creates a line that is clearly

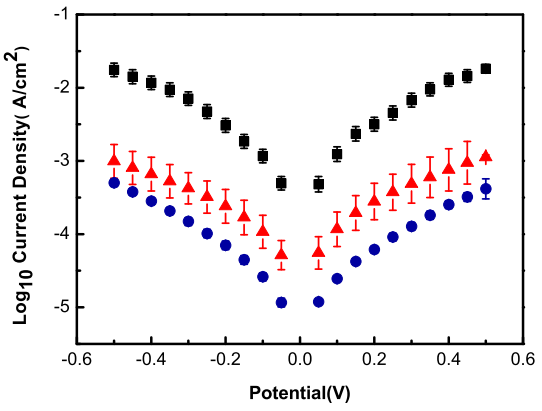

Figure 5. Log current-density *versus* potential plots for STAN electrodes fabricated from three different dithiols; SC12S (black squares), SC14S (red triangles), and SC16S (blue circles). Each plot is a log-average of at least 10 scans from five different STAN electrodes; the error bars are the variance.

visible to the naked eye.) We then placed the substrate in a home-built Faraday cage and grounded one of the electrodes using a small drop of EGaIn to connect the pad of silver paste to a tungsten probe. We contacted the other electrode by positioning a syringe with a sharp tip of EGaIn over the other pad of silver paste, bringing it in contact, and connecting the syringe to the electrometer (see Supporting Information). We observed four distinct behaviors: (i) no-contact, characterized by noisy, hysteretic currents in the pA regime; (ii) shorts, characterized by linear *I/V* curves with currents in the μA regime (see Supporting Information); (iii) poor-contact, for which we initially observed no-contact *I/V* curves, but could observe shorts after placing the EGaIn tip between the two silver pads (*i.e.*, over the gap, bridging the two electrodes); and (iv) working STAN electrodes, characterized by S-shaped *I/V* curves of reproducible, low-noise currents in the nA regime.

The *J/V* data for SC12S, SC14S, and SC16S are plotted in Figure 5. We calculated *J* (A/cm^2) using the maximum theoretical emission area of the height, defined by the ultramicrotome and the width, defined by the shadow mask and measured using a micrometer during fabrication (*i.e.*, E and D from Figure 2). Although the actual emission area may be smaller (due, for example, to deformation from mechanical stresses), this calculation assumes that any variations in size are systematic across all STANs and all three lengths of dithiols. The yields of working STAN electrodes are shown in Table 1; the average yield for STAN electrodes fabricated using dithiols is 58%. The lowest yield of 13% (for SC15CO$_2$H) and the highest yield of 71% (for SC14S) far exceed the ~1.2% that is typical for evaporated gold top-contacts (without a buffer layer).[22] While this result is counterintuitive in that longer dithiols should form more mechanically robust SAMs, the quality of the diamond knife can adversely impact

TABLE 1. The Yields of Working Junctions from STAN Electrodes Fabricated Using Various Thiols

thiol	no-contact (%)	shorted (%)	working (%)	devices
SC12S	8	25	67	12
SC14S	15	14	71	14
SC16S	28	36	36	14
SC15CO$_2$H	34	53	13	30

yields by introducing occasional breaks between where the silver paste is applied and the junction (*i.e.*, no-contacts) due to nicks in the cutting edge that can result from heavy usage. (Though likely not from fabricating the STANs in this paper, as gold films do not typically damage diamond knives.) We interpret poor-contacts and no-contacts as varying degrees of poor electrical contact between the silver paste and the electrodes—and not defects in the STAN electrodes themselves—because we were able to deliberately short the former, and we did not observe any discontinuities in any of the (dozens of) STANs that we examined by SEM; however, the aspect ratios of the STANs makes inspecting the entire length of more than a few of them impractical. Thus the frequency of these phenomena is not intrinsic to the fabrication process and can therefore be reduced. Shorts are most likely caused by the gold penetrating through defects in the SAM during deposition and are therefore intrinsic to the choice of SAM, metal, and deposition method. For dithiols, these defects can arise from the molecules forming loops by attaching to the gold through both thiols, which can be mitigated by fine-tuning the concentration and exposure time during the formation of the SAM.[32] Other types of defects can be mitigated by improving the quality of the template-stripped gold surface, using silver (SAMs of alkanethiolates pack more densely on silver than gold), improving the mechanical stability of the molecules *via* functionalization, and sharpening the diamond knives regularly.

The simplest approach to determining the dimensions of a tunneling gap that is too small to directly measure is to fit *I/V* curves of the gap to Simmons' approximation for a rectangular tunneling barrier,[33] however that requires removing the molecules from the STAN electrodes, as this approximation is not valid for alkanedithiols. Unfortunately we were unable to reliably remove the SAMs while retaining reproducible *I/V* data. Treatment with oxygen plasma, while resulting in intact STAN structures by SEM and TEM, yielded large spreads in the *I/V* curves (see Supporting Information). Exposure to piranha solution (H_2SO_4 in H_2O_2) yielded similar results. These spreads may simply be due to the oxidation of the pads of silver paste; the average resistance of single gold nanowires connected through pads of silver paste decreases from 2.57 to 1.58 kΩ after 15 min of exposure to oxygen plasma. Regardless, using another form of Simmons'

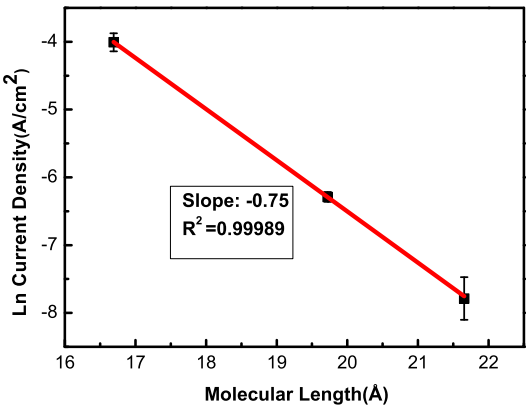

Figure 6. A plot of ln(*J*) *versus* length (Å) from the data in Figure 5 showing a linear fit (R^2 = 0.99) with a slope corresponding to $\beta = 0.75$ Å^{-1} (0.94 n_C^{-1}).

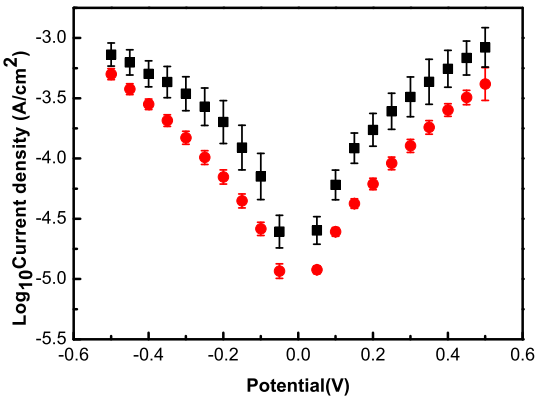

Figure 7. Log current−density *versus* potential plots for STAN electrodes fabricated from two different dithiols; SC15CO$_2$H (black squares) and SC16S (red circles). Each plot is a log-average of at least 20 scans from four different STAN electrodes. The lengths of the two thiols are within 0.7 Å of each other, implying that the slight difference in conductance is due to the differences in electronic coupling to gold between CO$_2$H and SH. The small magnitude of this difference implies that the gold electrode formed by depositing gold directly onto the SAM of SC15CO$_2$H forms a physisorbed and not a chemisorbed contact (*i.e.*, SH//Au, not S−Au).

approximation, $J = J_0 e^{-d\beta}$ where d is the width of the junction and J_0 is the theoretical value of J at $d = 0$, the characteristic tunneling decay, β, can be extracted from a linear fit of J as a function of the width of a junction (or number of carbons, n_C). This method provides not only a measure of the width of a junction, but also how precisely it can be controlled. And, since β has been determined for SAMs of alkanthiols[34] and dithiols[35] in a variety of systems, it offers strong evidence that the dithiols are defining the width of the junction and carrying the tunneling current; other possible carriers such as gold filaments or constriction points would yield a very different value for β. While there is a range of reported values of β for alkane backbones, the emerging consensus that it is 0.51−0.78 Å^{-1} (0.71−1.10 n_C^{-1}) at 200−500 mV.[24,25,36,37] Figure 6 is a plot of ln J at 500 mV (from the data in Figure 5) *versus* length (Å) for STAN electrodes containing SC16S, SC14S, and SC12S. From the slope of this plot, $\beta = 0.75$ Å^{-1} (0.94 n_C^{-1}) which is in excellent agreement with literature values. Thus, we conclude that the gap-width of the STAN structures is defined by the SAMs used as templates, that those SAMs remain intact after fabrication, and that the size of the gap can be defined with a resolution as small as 2.5 Å. Further evidence that the SAM not only remains intact, but undamaged, is shown in Figure 7 which is a plot of data from two STAN electrodes of approximately equal width; one fabricated using SC16S and one using SC15CO$_2$H, which is ∼0.7 Å shorter than SC16S—in principle, too small of a difference to detect by conductance measurements. Changing the headgroup from a thiol (that is either physi- or chemisorbed) to a carboxylic acid is, however, expected to produce detectible, but minor (and, importantly, nonexponential) changes in conductance (and the shape of the *J*/*V* curves). We observed exactly that—a slight change in the magnitude and shape of the *J*/*V* curves and a slight change in rectification. While we cannot derive the emission area from length-dependence measurements alone, the magnitudes of the values of J in Figure 5 are comparable to other SAM-based tunneling junctions in which one of the thiols of an alkanedithiol is electronically decoupled from the electrode.[35,38] This observation implies that the "top" electrode, formed by deposition onto the SAM, forms a physisorbed rather than chemisorbed interface with the thiol end-groups (*i.e.*, SH//Au, not S−Au).

CONCLUSIONS

Our overall goal with this work was to create a simple method for fabricating nanogaps on the order of the length scale of small molecules without any arduous lithography steps. Ideally, these nanogaps could be precisely defined by the thickness of a SAM—affording Angstrom-level control over the width of the gaps—that could later be removed and replaced with dithiols of similar lengths to form devices based on tunneling junctions. In this paper we have demonstrated the basic concept by fabricating STAN structures with gaps of 1.7−2.2 nm using only Nanoskiving and the hand-placement of mm-sized shadow masks to form gaps of ∼2 nm over areas of ∼50 μm^2. We can control all three dimensions of the STANs, pick-and-place them by hand, and they are directly electrically addressable using a light microscope to apply contact pads of silver paste (or using EGaIn tips). Length-dependent electrical measurements on intact alkanedithiols (before ashing the organics with oxygen plasma) clearly show that charge-transport is dominated by tunneling through the backbone of the SAM, demonstrating that the gaps are indeed defined by the lengths of the molecules in the SAMs. Thus, STAN electrodes offer an

exceedingly simple platform for directly fabricating tunneling junctions comprising SAMs that pack densely enough to withstand the deposition of gold. These electrodes offer five advantages over existing methods for fabricating nanogaps; (i) the resolution of the gap is at least 2.5 Å; (ii) no special equipment or infrastructure is needed to fabricate them—only an ultramicrotome; (iii) they are directly addressable as-fabricated, requiring no addition lithography steps; (iv) they can be fabricated on-demand (the epoxy blocks used to fabricate the STANs containing $SC15CO_2H$ were one year old) at the rate of about one per second; and (v) they can be placed onto almost any substrate with any orientation, and can be stacked and aligned. Although we were able to remove the SAM templates by plasma oxidation and exposure to piranha solution, and image them by electron microscopy, there was too much variance in the resulting electrical measurements to conclude that a uniform air-gap remained; however, the absence of shorts indicates that the gaps did not collapse. We are working on more reliable methods for removing the SAMs completely and for exchanging them with free thiols from solution, which will allow the construction of tunneling junctions from arbitrary (conjugated) thiols, in addition to those which are robust enough to serve as a template for STANs. Also, while this work focused on STANs of gold with gaps below 3 nm, larger gaps are readily accessible by using any number of other sacrificial spacers, and any material that is compatible with Nanoskiving—including conjugated polymers—can be substituted for gold.

METHODS

Materials. Epofix epoxy resin and hardener were purchased from Electron Microscopy Sciences. Gold with 99.9% purity was purchased from Schone Edelmetaal B.V. 1-Hexanethiol and 16-mercaptohexadecanoic were purchased from Sigma-Aldrich. 1,12-Dodecanedithiol, 1,14-tetradecanedithiol, or 1,16-hexadecanedithiol were furnished by Akkerman *et al.*[35] (Tridecafluoro-1,1,2,2,-tetrahydrooctyl)trichlorosilane was purchased from ABCR GmbH & Co. KG, and used as-is.

Fabrication. A 100 nm-thick layer of gold (in a home-built thermal deposition system) was deposited through a Teflon master (that defines the width of the resulting wires; 0.5 mm, 1 mm, or 1.5 mm) onto a technical-grade 3″ silicon wafer that had been treated in an air plasma cleaner (30 s) and then exposed to (tridecafluoro-1,1,2,2,-tetrahydrooctyl)trichlorosilane vapor for 1 h. The entire wafer was covered with 8.5 mL of Epofix epoxy prepolymer. After curing for three hours at 60, the gold layer was template-stripped by carefully peeling the epoxy from the wafer such that the gold remained attached to the cured epoxy. The template-stripped gold-on-epoxy was immersed in a 0.001 M solution of either 16-mercaptohexadecanoic, 1-hexanthiol, 1,12-dodecanedithiol, 1,14-tetradecanedithiol, or 1,16-hexadecanedithiol in ethanol overnight. After removing the epoxy substrate from the SAM-forming solution, rinsing it with ethanol, and drying it at 60 for 2 min, the same Teflon mask was placed back over the gold features, but laterally offset by ~80% of the shortest dimension of the Au features. A second 100 nm-thick layer of gold was then immediately deposited through the mask and the entire gold/SAM/gold/epoxy substrate was re-embedded in Epofix prepolymer (8.5 mL), which was then cured for 3 h at 60 °C. The gold features were cut out using a jeweler's saw (into ~4 × 10 mm pieces) and placed into separate wells in a polyethylene microtome mold (Electron Microscopy Sciences), which was then filled with Epofix prepolymer, and cured overnight at 60 °C.

To prepare for sectioning, a block was removed from the polyethylene mold, mounted in the ultramicrotome (Leica EM UC-6), and trimmed to the width of the diamond knife (2 or 4 mm Diatome Ultra 35°) using a razor blade that had been cleaned with ethanol to remove metal fragments. To fabricate a STAN structure, the block was sectioned with the ultramicrotome to either 100 nm at 1 mm/s or 50 nm at 0.6 mm/s. The epoxy sections containing the STANs were collected from the surface of the water in the reservoir of the knife either individually using a Perfect Loop (Electron Microscopy Sciences) or as ribbons (see Supporting Information) of several sections to an Si/SiO_2 (for SEM) or SiO_2 (for electrical measurements) substrate by placing the substrate under the surface of the water and raising it slowly. These sections were then dried at 60 °C to improve adhesion to the substrate. To remove the epoxy, the sections were treated with an O_2 plasma (15 min at 1 mbar was sufficient to remove all traces of the epoxy from 100 or 50 nm-thick sections).

Electrical Measurements. All electrical measurements were performed in a home-built Faraday cage using a Keithley 6430 source meter. The DUT (microtome section) was placed on a 0.5 cm-thick piece of glass to insulate it from ground, and held in place with a spring-loaded gold tip that was isolated from ground. The high and low inputs (see Supporting Information for a wiring diagram) were connected to a syringe filled with EGaIn and an articulated probe, respectively. The low input was grounded at the electrometer. In all cases, STAN electrodes driven to ±2 V shorted after one or two scans, producing linear *I*/*V* curves and mA currents (see Supporting Information). This collapse is induced by the electrostatic forces resulting from the $\sim 10^7$ V/cm electric field, and is the expected behavior of SAMs of alkanethiolates sandwiched between deformable electrodes. If the tunneling current was the result of a nick in the wire, rather than the gap between the electrodes, increasing the voltage to ±2 would instead induce electromigration in the nanowire, resulting in the loss of current rather than a short.

Imaging. SEM images were acquired with a Jeol JSM 7000F scanning electron microscope operated at 30 kV with a working distance of 10 mm. Transmission electron microscopy was performed on a Philips CM10 transmission electron microscope operating at an accelerating voltage of 100 kV.

Conflict of Interest: The authors declare no competing financial interest.

Acknowledgment. This work is part of the Joint Solar Programme (JSP) of the Stichting voor Fundamenteel Onderzoek der Materie FOM, which is supported financially by Nederlandse Organisatie voor Wetenschappelijk Onderzoek (NWO). This work is cofinanced by Nuon Helianthos. We thank Dr. Marc Stuart for assistance with the TEM measurements.

Supporting Information Available: A detailed description of Nanoskiving, photographs of some STAN electrodes, and control experiments. This material is available free of charge *via* the Internet at http://pubs.acs.org.

REFERENCES AND NOTES

1. Li, T.; Hu, W.; Zhu, D. Nanogap Electrodes. *Adv. Mater.* **2010**, *22*, 286–300.

2. Carroll, R.; Gorman, C. The Genesis of Molecular Electronics. *Angew. Chem., Int. Ed.* **2002**, *41*, 4378–4400.
3. Reed, M. A.; Zhou, C.; Muller, C. J.; Burgin, T. P.; Tour, J. M. Conductance of a Molecular Junction. *Science* **1997**, *278*, 252–254.
4. Chen, W.; Ahmed, H.; Nakazoto, K. Nanoscale Metallic Islands in a Lateral Nanostructure. *Appl. Phys. Lett.* **1995**, *66*, 3383–3384.
5. Morpurgo, A. F.; Marcus, C. M.; Robinson, D. B. Controlled Fabrication of Metallic Electrodes with Atomic Separation. *Appl. Phys. Lett.* **1999**, *74*, 2084–2086.
6. Paska, Y.; Haick, H. Systematic Cross-Linking Changes within a Self-Assembled Monolayer in a Nanogap Junction: A Tool for Investigating the Intermolecular Electronic Coupling. *J. Am. Chem. Soc.* **2010**, *132*, 1774–1775.
7. Park, J.; Pasupathy, A. N.; Goldsmith, J. I.; Chang, C.; Yaish, Y.; Petta, J. R.; Rinkoski, M.; Sethna, J. P.; Abruna, H. D.; McEuen, P. L.; Ralph, D. C.; *et al.* Coulomb Blockade and the Kondo Effect in Single-Atom Transistors. *Nature* **2002**, *417*, 722–725.
8. Nagase, T.; Kubota, T.; Mashiko, S. Fabrication of Nano-gap Electrodes for Measuring Electrical Properties of Organic Molecules Using a Focused Ion Beam. *Thin Solid Films* **2003**, *438*−*439*, 374–377.
9. Kubatkin, S.; Danilov, A.; Hjort, M.; Cornil, J.; Brédas, J.-L.; Stuhr-Hansen, N.; Hedegård, P.; Bjørnholm, T. Single-Electron Transistor of a Single Organic Molecule with Access to Several Redox States. *Nature* **2003**, *425*, 698–701.
10. Notargiacomo, A.; Foglietti, V.; Cianci, E.; Capellini, G.; Adami, M.; Faraci, P.; Evangelisti, F.; Nicolini, C. Atomic Force Microscopy Lithography as a Nanodevice Development Technique. *Nanotechnology* **1999**, *10*, 458–463.
11. Qin, L.; Park, S.; Huang, L.; Mirkin, C. A. On-Wire Lithography. *Science* **2005**, *309*, 113–115.
12. Hatzor, A.; Weiss, P. S. Molecular Rulers for Scaling Down Nanostructures. *Science* **2001**, *291*, 1019–1020.
13. Xu, Q.; Rioux, R. M.; Dickey, M. D.; Whitesides, G. M. Nanoskiving: A New Method To Produce Arrays of Nanostructures. *Acc. Chem. Res.* **2008**, *41*, 1566–1577.
14. Xu, Q.; Rioux, R. M.; Whitesides, G. M. Fabrication of Complex Metallic Nanostructures by Nanoskiving. *ACS Nano* **2007**, *1*, 215–227.
15. Lipomi, D. J.; Martinez, R. V.; Whitesides, G. M. Use of Thin Sectioning (Nanoskiving) To Fabricate Nanostructures for Electronic and Optical Applications. *Angew. Chem., Int. Ed.* **2011**, *50*, 8566–8583.
16. Lipomi, D. J.; Ilievski, F.; Wiley, B. J.; Deotare, P. B.; Lončar, M.; Whitesides, G. M. Integrated Fabrication and Magnetic Positioning of Metallic and Polymeric Nanowires Embedded in Thin Epoxy Slabs. *ACS Nano* **2009**, *3*, 3315–3325.
17. Lipomi, D. J.; Kats, M. A.; Kim, P.; Kang, S. H.; Aizenberg, J.; Capasso, F.; Whitesides, G. M. Fabrication and Replication of Arrays of Single- or Multicomponent Nanostructures by Replica Molding and Mechanical Sectioning. *ACS Nano* **2010**, *4*, 4017–4026.
18. Lipomi, D. J.; Chiechi, R. C.; Dickey, M. D.; Whitesides, G. M. Fabrication of Conjugated Polymer Nanowires by Edge Lithography. *Nano Lett.* **2008**, *8*, 2100–2105.
19. Lipomi, D. J.; Chiechi, R. C.; Reus, W. F.; Whitesides, G. M. Laterally Ordered Bulk Heterojunction of Conjugated Polymers: Nanoskiving a Jelly Roll. *Adv. Funct. Mater.* **2008**, *18*, 3469–3477.
20. Akkerman, H. B.; de Boer, B. Electrical Conduction through Single Molecules and Self-Assembled Monolayers. *J. Phys.: Condens. Phys.* **2007**, *20*, 013001–013021.
21. McCarty, G. S. Molecular Lithography for Wafer-Scale Fabrication of Molecular Junctions. *Nano Lett.* **2004**, *4*, 1391–1394.
22. Kim, T.; Wang, G.; Lee, H.; Lee, T. Statistical Analysis of Electronic Properties of Alkanethiols in Metal−Molecule−Metal Junctions. *Nanotechnology* **2007**, *18*, 315204–315212.
23. Macroscopic defects, which can be catastrophic for any deposition technique, are trivial to circumvent by skiving the few microns from the block that contain a defect.
24. Thuo, M. M.; Reus, W. F.; Nijhuis, C. A.; Barber, J. R.; Kim, C.; Schulz, M. D.; Whitesides, G. M. Odd−Even Effects in Charge Transport across Self-Assembled Monolayers. *J. Am. Chem. Soc.* **2011**, *133*, 2962–2975.
25. Weiss, E. A.; Chiechi, R. C.; Kaufman, G. K.; Kriebel, J. K.; Li, Z.; Duati, M.; Rampi, M. A.; Whitesides, G. M. Influence of Defects on the Electrical Characteristics of Mercury-Drop Junctions: Self-Assembled Monolayers of *n*-Alkanethiolates on Rough and Smooth Silver. *J. Am. Chem. Soc.* **2007**, *129*, 4336–4349.
26. Dickey, M.; Lipomi, D.; Bracher, P.; Whitesides, G. Electrically Addressable Parallel Nanowires with 30 nm Spacing from Micromolding and Nanoskiving. *Nano Lett.* **2008**, *8*, 4568–4573.
27. Weiss, E. A.; Kaufman, G. K.; Kriebel, J. K.; Li, Z.; Schalek, R.; Whitesides, G. M. Si/SiO_2- Templated Formation of Ultraflat Metal Surfaces on Glass, Polymer, and Solder Supports: Their Use as Substrates for Self-Assembled Monolayers. *Langmuir* **2007**, *23*, 9686–9694.
28. Chiechi, R. C.; Weiss, E. A.; Dickey, M. D.; Whitesides, G. M. Eutectic Gallium−Indium (EGaIn): A Moldable Liquid Metal for Electrical Characterization of Self-Assembled Monolayers. *Angew. Chem.* **2008**, *47*, 142–144.
29. Powell, R.; Francombe, M. H.; Ulman, A. *Thin Films*; Self-Assembled Monolayers of Thiols, Vol. 24; Academic Press: San Diego, CA, 1998.
30. Thiols do not necessarily form gold−thiolate bonds during the deposition of gold, rather thiols have a higher surface free-energy than methyl groups.
31. Lee, B. Y.; Heo, K.; Schmucker, A. L.; Jin, H. J.; Lim, J. K.; Kim, T.; Lee, H.; Jeon, K.-S.; Suh, Y. D.; Mirkin, C. A.; Hong, S.; *et al.* Nanotube-Bridged Wires with Sub-10 nm Gaps. *Nano Lett.* **2012**, *12*, 1879–1884.
32. Akkerman, H.; Kronemeijer, A.; van Hal, P.; de Leeuw, D.; Blom, P. M.; de Boer, B. Assembled-Monolayer Formation of Long Alkanedithiols in Molecular Junctions. *Small* **2008**, *4*, 100–104.
33. Simmons, J. G. Generalized Formula for the Electric Tunnel Effect between Similar Electrodes Separated by a Thin Insulating Film. *Appl. Phys. Lett.* **1963**, *34*, 1793–1803.
34. Slowinski, K.; Fong, H. K. Y.; Majda, M. Mercury−Mercury Tunneling Junctions. 1. Electron Tunneling across Symmetric and Asymmetric Alkanethiolate Bilayers. *J. Am. Chem. Soc.* **1999**, *121*, 7257–7261.
35. Akkerman, H.; Blom, P.; de Leeuw, D. M.; Boer, B. D. Towards Molecular Electronics with Large-Area Molecular Junctions. *Nature* **2006**, *441*, 69–72.
36. Song, H.; Kim, Y.; Jeong, H.; Reed, M. A.; Lee, T. Coherent Tunneling Transport in Molecular Junctions. *J. Phys. Chem. C* **2010**, *114*, 20431–20435.
37. Wang, W.; Lee, T.; Reed, M. Mechanism of Electron Conduction in Self-Assembled Alkanethiol Monolayer Devices. *Phys. Rev. B* **2003**, *68*, 035416.
38. Sek, S.; Bilewicz, R.; Slowinski, K. Electrochemical Wiring of α,ω-Alkanedithiol Molecules into an Electrical Circuit. *Chem. Commun.* **2004**, 404–405.